KCNH2$_{A561V}$ Heterozygous Mutation Inhibits KCNH2 Protein Expression via The Activation of UPR Mediated by ATF6

Bangsheng CHEN[1]*, Lian TAN[2]*, Danqi CHEN[2], Xinghou WANG[1], Jiequan LIU[1], Xiaoyan HUANG[3], Ying WANG[3], Shuaishuai HUANG[4], Feiyan MAO[5], Jiangfang LIAN[3]

** These authors contributed equally to this work.*

[1]Emergency Medical Center, Ningbo Yinzhou No. 2 Hospital, Ningbo, Zhejiang, China, [2]Intensive Care Unit, Ningbo Yinzhou No. 2 Hospital, Ningbo, Zhejiang, China, [3]Department of Cardiology, Ningbo Medical Center LiHuiLi Hospital, Ningbo, Zhejiang, China, [4]Laboratory of Renal Carcinoma, Ningbo Yinzhou No. 2 Hospital, Ningbo, Zhejiang, China, [5]Department of General Surgery, Ningbo No. 2 Hospital, Ningbo, Zhejiang, China

Received March 12, 2023
Accepted May 26, 2023

Summary

The potassium channel protein KCNH2 is encoded by *KCNH2* gene, and there are more than 300 mutations of *KCNH2*. Unfolded protein response (UPR) is typically initiated in response to an accumulation of unfolded and/or misfolded proteins in the endoplasmic reticulum (ER). The present study aimed to explore the UPR process and the role of activating transcription factor 6 (ATF6) in the abnormal expression of potassium voltage-gated channel subfamily H member 2 (KCNH2)$_{A561V}$. The wild-type (wt) KCNH2 and A561V mutant KCNH2 was constructed with his-tag. The 293 cells were used and divided into KCNH2$_{wt}$+KCNH2$_{A561V}$, KCNH2$_{wt}$ and KCNH2$_{A561V}$ groups. The expression levels of ATF6 and KCNH2 in different groups were detected by Western blotting, reverse transcription-quantitative PCR, immunofluo-rescence and immuno-coprecipitation assays. The protein types and abundance of immuno-coprecipitation samples were analyzed by mass spectrometry. The proteomic analysis of the mass spectrometry results was carried out by using the reactome database and GO (Gene Ontology) tool. The mRNA expression levels of *KCNH2* and *ATF6* in the KCNH2$_{wt}$+KCNH2$_{A561V}$ group were higher compared with the KCNH2$_{A561V}$ group. However, the full-length protein expression of ATF6 was inhibited, indicating that ATF6 was highly activated and a substantial number of ATF6 was sheared in KCNH2$_{wt}$+KCNH2$_{A561V}$ group compared with control group. Furthermore, A561V-KCNH2 mutation leading to the accumulation of the immature form of KCNH2 (135 kDa bands) in ER, resulting in the reduction of the ratio of 155 kDa/135 kDa. In addition, the abundance of UPR-related proteins in the KCNH2$_{A561V}$ group was higher compared with the KCNH2$_{wt}$+KCNH2$_{A561V}$ group. The 'cysteine biosynthetic activity' of GO:0019344 process and the 'positive regulation of cytoplasmic translation activity' of GO:2000767 process in the KCNH2$_{A561V}$ group were higher compared with the KCNH2$_{wt}$+KCNH2$_{A561V}$ group. Hence, co-expression of wild-type and A561V mutant KCNH2 in 293 cells activated the UPR process, which led to the inhibition of protein translation and synthesis, in turn inhibiting the expression of KCNH2. These results provided a theoretical basis for clinical treatment of Long QT syndrome.

Key words

KCNH2 • Long QT syndrome • ATF6 • Unfolded protein response • Endoplasmic reticulum stress

Corresponding authors

F. Mao, Department of General Surgery, Ningbo No.2 Hospital, Ningbo, China. E-mail: 103875411@qq.com and J. Lian, Department of Cardiology, Ningbo Medical Center LiHuiLi Hospital, Xingning Road, Ningbo 315100, China. E-mail: hjmpin@163.com

Introduction

Long QT syndrome (LQTS) refers to a group of clinical syndromes caused by an abnormal repolarization or the phase III of action potential of the heart [1]. LQTS is attributed to a decrease in the number of functional potassium channels on the cardiac cell membrane, which

weakens the rapid activation of the delayed rectifier potassium current. LQTS includes hereditary long QT syndrome (hLQTS) and acquired LQTS (aLQTS), hLQTS and aLQTS have similar clinical manifestations [2,3]. QT interval prolongation and arrhythmia can be detected *via* electrocardiogram and torsade de pointes; clinical syncope and cardiac arrest can be observed [4]. Currently, hLQTS have 13 pathogenic genes, which can be divided into LQT1-LQT13 subtypes [5]. LQT2 [potassium voltage-gated channel subfamily H member 2 (KCNH2) mutation] is the main type of mutations in patients with LQTS in China [6]. The potassium channel protein KCNH2 is encoded by KCNH2, which has >300 mutations [7]. The LQT2 caused by the mutations of KCNH2 accounts for ~45 % of the total mutations [8,9], and the main mutation type is missense mutation. A561V is a common and classical dominant LQTS pathogenic mutation of KCNH2 [10]. A561V mutation causes the misfolding of KCNH2, and the mutant and wild-type proteins form a heterozygous ion channel with a reduced function, it also inhibits the protein expression of the mature KCNH2 [11-13]. However, studies on the role of endoplasmic reticulum stress (ERS) or unfolded protein response (UPR) in the dysfunction of the A561V mutation of KCNH2 are limited [14].

The ER is essential for intracellular calcium storage, lipid biosynthesis, protein folding and assembly. ERS can be induced by the imbalance of protein and calcium homeostasis caused by the accumulation of misfolded or unfolded proteins in the ER [15]. In addition, ERS can trigger UPR [16]. The UPR-related signaling pathway is mainly mediated by pancreatic ER kinase (PKR)-like ER kinase (PERK), consequently activating transcription factor 6 (ATF6) and inositol requiring enzyme 1 (IRE-1), which are 3 important UPR sensors [17]. UPRs can feedback the protein folding in ER lumen to the cytoplasm and the nucleus, stimulate the expression of ER-resident proteins and folding-related enzymes such as PERK and ATF6 and enhance the ability of the ER lumen to process protein folding. UPRs can also reduce protein biosynthesis in the ER by temporarily downregulating or causing cessation of protein synthesis-related transcription and translation [18,19], or by increasing the ability of unfolded protein clearance by enhancing the degradation of ER proteins, hence restoring the internal balance of cells [20]. Activated ATF6 is a transcription factor upregulating UPRs [21]. $KCNH2_{A561V}$ may prevent the efficient folding of KCNH2, causing UPRs induction and reducing the level of mature KCNH2 [22-24].

The present study aimed to explore the UPR process and the role of ATF6 in the abnormal expression of $KCNH2_{A561V}$, which could provide a therapeutic pathway for Long QT syndrome, and theoretical basis for clinical treatment of Long QT syndrome.

Materials and Methods

Cell culture and transfection

293 cells (American type culture collection, ATCC) were cultured using MEM medium supplemented with 10 % FBS (Gibco; Thermo Fisher Scientific, Inc.), 1 % penicillin and 1 % streptomycin at 37 °C and 5 % CO_2 for 24 h. The cells were divided into control (normal 293 cells), KCNH2 (wild-type) wt (transiently expression of wild-type KCNH2 in 293 cells), $KCNH2_{A561V}$ (transfection of A561V mutant KCNH2 in 293 cells), and $KCNH2_{wt}$+$KCNH2_{A561V}$ groups (transfection of A561V mutant KCNH2 and wild-type KCNH2 in 293 cells). Lentiviral plasmids KCNH2 (wild-type) wt and $KCNH2_{A561V}$ were purchased from General Bio Co., Ltd. and 2.5 µg plasmid was used for transfection. Transfection was performed using a Lipofectamine 3000® kit (Invitrogen; Thermo Fisher Scientific Inc.) in accordance with the manufacturer's instructions. After 4 h of transfection, 2 ml of complete medium with 10 % serum was added into the plate and cultured for 48 h.

Reverse transcription-quantitative (RT-q) PCR

Total RNA was extracted from cells using a TRIzol® (Invitrogen; Thermo Fisher Scientific Inc.) reagent kit. The purity and concentration of RNA were detected using a NanoDrop™ 1000 spectrophotometer (Thermo Fisher Scientific Inc.). RT2 First Strand kit (Qiagen GmbH) was used to reverse transcribe RNA into cDNA and qPCR was performed using a SYBR Green PCR kit (Qiagen GmbH) in accordance with the manufacturer's protocol with an ABI StepOne Plus system (Applied Biosystems; Thermo Fisher Scientific, Inc.). The PCR conditions were as follows: 95 °C for 10 min, followed by 40 cycles of 95 °C for 10 s and 60 °C for 40 s. Quantification was performed using the $2^{-\Delta\Delta Cq}$ method [25]. GAPDH was used as the internal control. The primers used were listed in Table 1.

Western blotting

Proteins were extracted from the cells in all groups. In brief, after being rinsed with PBS for 3 times,

Table 1. RT-qPCR primers.

Gene	Sequence (5'→3')	Primer length, bp	Product length, bp	Annealing temperature, °C
KCNH2 F	ACTACTTCAAGGGCTGGTTCC	20	313	59.1
KCNH2 R	GGTTTGCCTATCTGGTCGC	19		
ATF6 F	GCTGGATGAAGATTGGGATT	20	220	57.2
ATF6 R	TGGAGAAAGTGGCTGAGGTT	20		
GAPDH F	AGCCACATCGCTCAGACAC	19	66	58.2
GAPDH R	GCCCAATACGACCAAATCC	19		

KCHN2, potassium voltage-gated channel subfamily H member 2; ATF6, activating transcription factor 6; R, reverse; F, forward; RT-q, reverse transcription-quantitative.

the cells were harvested and proteins were extracted using RIPA buffer (Thermo Fisher Scientific Inc.). Proteins were quantified using a bicinchoninic acid (BCA) kit and loaded in 10 % SDS-PAGE gels (20 µg/lane). The proteins were then electrotransferred to a PVDF membrane. The PVDF membrane was rinsed with Methanol for 5 min and placed in TBST blocking buffer containing 5 % (w/v) skimmed milk powder at room temperature for 1 h. The samples were incubated at 4 °C overnight with the following primary antibodies: Mouse Monoclonal Anti-GAPDH (1:2,000; Cat. no. TA-08; Origene Technologies Inc.); Mouse Monoclonal Anti-ATF6 (1:1,000; Cat. no. ab122897; Abcam); and Rabbit Anti-KCNH2 (1:400; Cat. no. APC-062; Alomone Labs). The membrane was then rinsed with TBST 4 times and then incubated at room temperature for 2 h with horseradish peroxidase-labeled goat anti-mouse IgG (H+L) secondary antibody (1:10,000; Cat. no. 32260; Thermo Fisher Scientific, Inc.). Images were collected using an ImageQuant LAS 4000 imaging station (GE Healthcare) and quantification was performed using Quantity One software (v4.6, Bio-Rad Laboratories, Inc.).

Immunofluorescence

293 cells were harvested when they were 80-90 % confluent (10^4/ml) and washed with PBS 3 times. The cells were then fixed with 4 % paraformaldehyde for 15 min at room temperature. Subsequently, 0.5 % Triton X-100 was added for 20 min at room temperature. After 30 min of blocking with 5 % BSA at 37 °C, the cells were incubated with a FITC-conjugated primary antibody goat anti-rabbit IgG (1:500; Cat. no. CW0114S; CWBio) at 4 °C overnight. The Cy3 conjugated secondary antibody goat anti-mouse IgG (1:200; Cat. no. CW0145S; ComWin Biotech Co., Ltd.) diluted with blocking buffer was used to stain sections at 37 °C for 30 min. DAPI was added and incubated in dark for 5 min. The samples were sealed with 50 % glycerol and observed under a fluorescence microscope (Leica Microsystems GmbH; magnification, ×200) with ImageJ software (v1.37; National Institutes of Health). Red fluorescence indicated the target protein and blue fluorescence indicated the nucleus.

Co-immunoprecipitation and proteomic analysis

$KCNH2_{A561V}$ and $KCNH2_{wt}$+$KCNH2_{A561V}$ group lysates were used as samples, and immunoprecipitation was carried out using the mouse anti-His tag antibody (Cat. no. TA-02; Origene Technologies Inc.) and A561V mutant KCNH2 protein as a bait protein. Plasmid backbone was pCDNA3.1(+) (Miaoling Bio Ltd., Wuhan, China). Lipofectamine®3000 (Invitrogen; Thermo Fisher Scientific Inc.) was used for transfection at 37 °C for 48 h in accordance with the manufacturer's instructions, and then subsequent experimentation was performed. In brief, the cells were split (RIPA lysis buffer, Sigma-Aldrich), and 20 µl of the cell lysate was diluted with co-IP buffer 10 times as an input. A co-immunocoprecipitation system was prepared with 200 µl of cell lysate, 5 µl mouse anti-His tag antibody (Cat. no. TA-02; Origene Technologies Inc.), 20 µl of immunomagnetic suspension and 5 µl of the mixed protease inhibitor and co-IP buffer in a 1.5 ml Eppendorf tube and they were mixed on a rotary mixer overnight. The tube was placed on a magnetic tube rack. The Protein A/G Agarose beads (Cat. 36403ES03, Yeasen Biotech Co., Ltd., Shanghai, China) were attached onto the tube wall and the supernatant was removed. The beads were washed with co-IP buffer (Cat. no. 26149; Thermo Fisher Scientific, Inc.) and PBS, 200 µl of elution buffer was added and the sample was mixed for 10 min at room temperature, 50 µl of Tris buffer was added to eluent to the neutralize the pH value

and co-IP protein samples were obtained. SDS-PAGE electrophoresis was performed. The target band was cut off and fixed with 40 % ethanol and 10 % acetic acid for 30 min at room temperature. The sample was stained with R250 Coomassie brilliant blue at room temperature for 10 min. The band was cut into rubber particles with a diameter of 1-2 mm with a blade and placed into 1.5 ml EP tubes. The particles were washed thrice with 200 µl MilliQ (EMD Millipore) for 10 min at each time. Subsequently, 100 µl of ACN was added for dehydration and 10 mM DTT was added for reduction at 37 °C for 1 h. The particles were alkylated with 30 mM IAA and the peptides were extracted. The protein types and abundance were analyzed by LC-MS (Thermo EASY nLC, Thermo Scientific Orbitrap Fusion Lumos, USA, positive ionization; resolution: 120,000, AGC target: 4e5, Maximum IT: 50 ms, scan range: 350 to 1550 m/z, nitrogen gas temperature 350 °C, nebulizer pressure 40 psi and flow rate 10 l/min. The mass spectrometry results were subjected to proteomic analysis by using the reactor database and Gene Ontology (GO) tool. Thermogram of UPR and cardiac production related proteins could be obtained.

Differentially expressed gene

There were 92 UPR (R-HSA-380994) related proteins and 140 cardiac conduction-related proteins (R-HSA-5576891) in reactome database (https://reactome.org/) screened in the present study. The screened differentially expressed genes were enriched by gene ontology (GO) analysis.

Statistical analysis

Statistical analysis was performed using SPSS 19.0 (IBM Corp.) software. All experiments were repeated three times. All data are presented as the mean ± standard deviation. One-Way ANOVA test and *post hoc* Sidak's multiple comparisons test were performed. $P<0.05$ was considered to indicate a statistically significant difference.

Results

ATF6 and KCNH2 expression levels in different groups of treated 293 cells

As shown in Figure 1A, *KCNH2* expression in different groups of 293 cells was evaluated using RT-qPCR. In particular, the mRNA expression level of *KCNH2* in the 293 cells (control group) was extremely low. However, in the other groups, this expression increased, the highest and a significant difference was observed in the $KCNH2_{wt}$+$KCNH2_{A561V}$ group ($P<0.05$; Fig. 1A). Additionally, *ATF6* mRNA expression increased and only the changes seen in the $KCNH2_{wt}$+$KCNH2_{A561V}$ group were significant compared with that of the control group ($P<0.05$; Fig. 1B). As

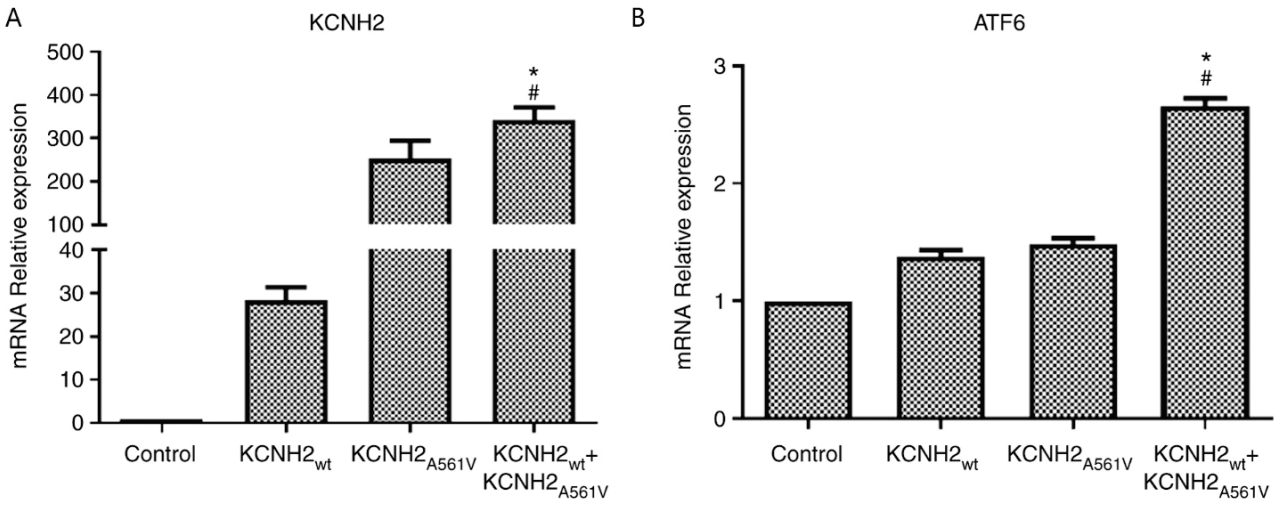

Fig. 1. *KCNH2* mRNA and *ATF6* mRNA expression in different groups. (**A**) *KCNH2* mRNA expression. (**B**) *ATF6* mRNA expression. *KCNH2* mRNA expression level in 293 cells was very low. Compared with the control group, *KCNH2* mRNA expression increased in the $KCNH2_{wt}$, $KCNH2_{A561V}$ and the $KCNH2_{wt}$+$KCNH2_{A561V}$ groups. *ATF6* mRNA expression increased in the $KCNH2_{wt}$, $KCNH2_{A561V}$ and the $KCNH2_{wt}$+$KCNH2_{A561V}$ groups. * $P<0.05$, $KCNH2_{wt}$+$KCNH2_{A561V}$ vs. $KCNH2_{wt}$; # $P<0.05$, $KCNH2_{wt}$+$KCNH2_{A561V}$ vs. $KCNH2_{A561V}$. KCHN2, potassium voltage-gated channel subfamily H member 2; ATF6, activating transcription factor 6; control, normal 293 cells; $KCNH2_{wt}$, 293 cells with transiently expression of wild-type KCNH2; $KCNH2_{A561V}$, transfection of A561V mutant KCNH2 in 293 normal cells; $KCNH2_{wt}$+$KCNH2_{A561V}$ groups, transfection of A561V mutant KCNH2 and wild-type KCNH2 plasmids into 293 cells; wt, wild-type; RT-q, reverse transcription-quantitative.

shown in Figure 2A, the protein expression of ATF6 decreased in the $KCNH2_{wt}$, $KCNH2_{A561V}$ and $KCNH2_{wt}$+$KCNH2_{A561V}$ groups and the lowest value was observed in the $KCNH2_{wt}$+$KCNH2_{A561V}$ group compared with the control group. Furthermore, the KCNH2 protein has two bands, the mature form at 155 kDa and the immature form at 135 kDa. Compared with the $KCNH2_{wt}$ group, the mature form of KCNH2 increased slightly in $KCNH2_{wt}$+$KCNH2_{A561V}$ group and almost disappeared in $KCNH2_{A561V}$ group, however, the protein expression level of immature KCNH2 increased, and the highest value was detected in the $KCNH2_{wt}$+$KCNH2_{A561V}$ group (Fig. 2C).

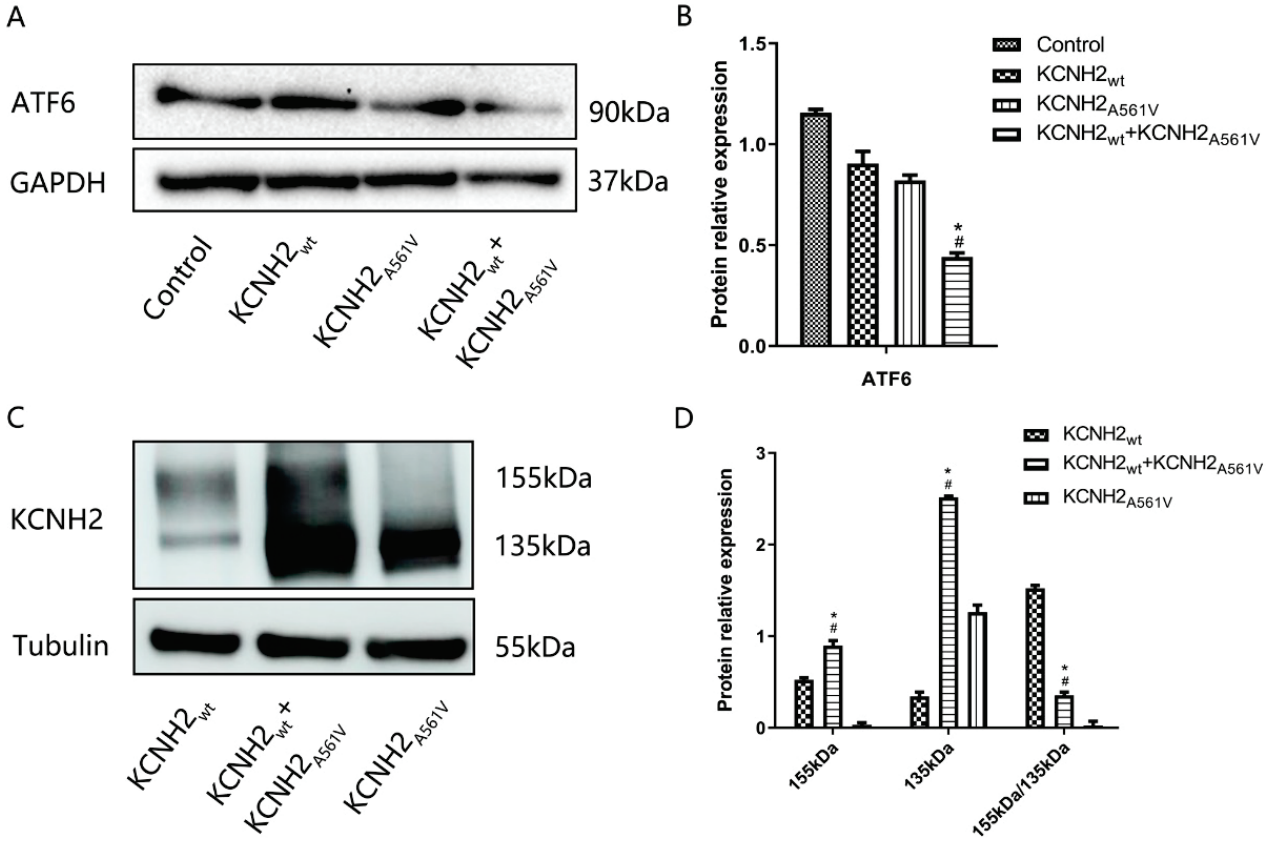

Fig. 2. KCNH2 and ATF6 protein expression in different groups detected by Western blotting. (**A**) Western blot of ATF6 in the indicated groups. (**B**) Quantitative Western blot analysis. The protein expression of ATF6 decreased in the $KCNH2_{wt}$, $KCNH2_{A561V}$ and $KCNH2_{wt}$+$KCNH2_{A561V}$ groups. (**C**) Western blot of KCNH2 in the indicated groups. (**D**) Quantification of densitometries of Western blot bands. Compared with the $KCNH2_{wt}$ group, the expression of immature KCNH2 (135 kDa bands) increased significantly in the $KCNH2_{A561V}$ and $KCNH2_{wt}$+$KCNH2_{A561V}$ groups. However, the mature form of KCNH2 (155 kDa bands) almost disappeared in $KCNH2_{A561V}$ group, and has a slightly increase in $KCNH2_{wt}$+$KCNH2_{A561V}$ group, but has a minimum function due to dominant negative suppression as reported previously. Furthermore, the ratio of 155 kDa to 135 kDa decreased significantly in $KCNH2_{A561V}$ and $KCNH2_{wt}$+$KCNH2_{A561V}$ groups compared with $KCNH2_{wt}$. * $P<0.05$, $KCNH2_{wt}$+$KCNH2_{A561V}$ vs. $KCNH2_{wt}$; # $P<0.05$ $KCNH2_{wt}$+$KCNH2_{A561V}$ vs. $KCNH2_{A561V}$. KCHN2, potassium voltage-gated channel subfamily H member 2; ATF6, activating transcription factor 6; control, normal 293 cells; $KCNH2_{wt}$, 293 cells with transiently expression of wild-type KCNH2; $KCNH2_{A561V}$, transfection of A561V mutant KCNH2 in 293 normal cells; $KCNH2_{wt}$+$KCNH2_{A561V}$ groups, transfection of A561V mutant KCNH2 and wild-type KCNH2 plasmids into 293 cells.

The immunofluorescence results for KCHN2 demonstrated no significant difference in the fluorescence between the control group and the $KCNH2_{wt}$ groups (Fig. 3). The growth state of the cells in the $KCNH2_{A561V}$ group and the $KCNH2_{wt}$+$KCNH2_{A561V}$ group was lower compared with the control and $KCNH2_{wt}$ groups (Fig. 3).

The mRNA expression level of *KCNH2* increased significantly in $KCNH2_{wt}$+$KCNH2_{A561V}$ and $KCNH2_{A561V}$ groups compared with the $KCNH2_{wt}$ group, whereas our study showed that a large amount of immature KCNH2 was accumulated in ER, resulting in a reduction of mature and functional KCNH2 on plasma membrane in $KCNH2_{wt}$+$KCNH2_{A561V}$ and $KCNH2_{A561V}$

groups. Besides, the expression of the uncut ATF6 was lower in the $KCNH2_{A561V}$ and $KCNH2_{wt}$+ $KCNH2_{A561V}$ groups, which suggested that the UPR activity increased in these two groups. Hence, the mature form of KCNH2 protein expression was inhibited in $KCNH2_{wt}$+$KCNH2_{A561V}$ and $KCNH2_{A561V}$ groups, indicating the presence of a strong UPR. UPRs can become cytotoxic and induce apoptosis [26]. Overall, strong UPRs in these cell models may promote apoptosis.

Proteomic analysis results

A total of 92 UPR (R-HSA-380994)-related proteins are listed in the reactor database. Among them, 32 were detected in the present study. A total of 7 RNA exosome complex proteins (EXOS1-9) were observed in the $KCNH2_{A561V}$ group, whereas only 4 proteins were found in the $KCNH2_{wt}$+ $KCNH2_{A561V}$ group (Fig. 4). Of the 140 proteins related to cardiac conduction (R-HSA-5576891), 11 were found in the present study (Fig. 4). The ratio of the abundance of the KCNH2 protein in the $KCNH2_{wt}$+$KCNH2_{A561V}$ group and the $KCNH2_{A561V}$ group was 0.772. The abundance of the UPR-related protein in the $KCNH2_{A561V}$ group was higher compared with the $KCNH2_{wt}$+$KCNH2_{A561V}$ group. No significant difference was observed in the proteins related to cardiac conduction between the $KCNH2_{wt}$+$KCNH2_{A561V}$ group and the $KCNH2_{A561V}$ group (Fig. 4).

Differentially expressed genes were screened under the condition that the abundance in the $KCNH2_{A561V}$ group was 8 times higher compared with the $KCNH2_{wt}$+$KCNH2_{A561V}$ group. The highly prominent and specific biological processes and the corresponding enriched genes subjected to the gene ontology classification and enrichment analysis of differentially expressed genes were listed in Table 2. The ranking list of GO analysis according to the false discovery rate (FDR) were presented in Table 3.

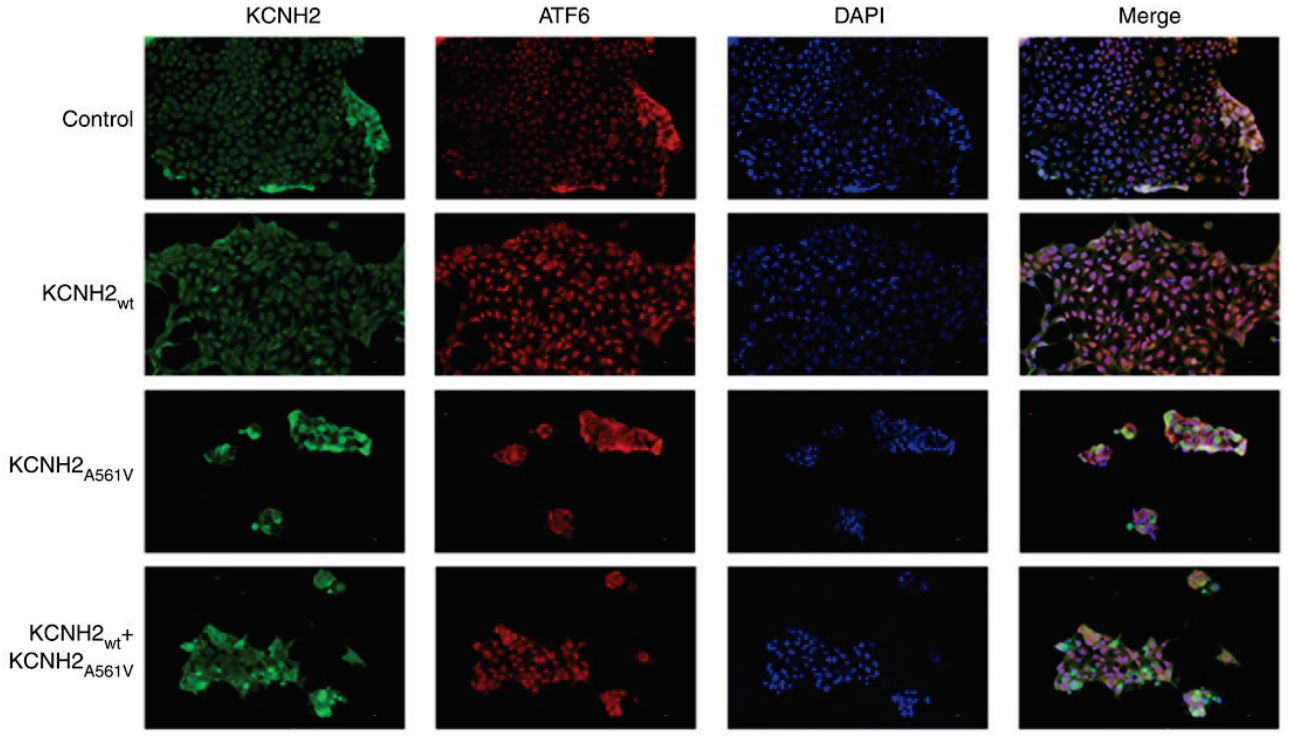

Fig. 3. KCNH2 and ATF6 expression detected by immunofluorescence. There was no significant difference in the fluorescence between the control and the $KCNH2_{wt}$ groups. The cells in the $KCNH2_{A561V}$ and the $KCNH2_{wt}$+$KCNH2_{A561V}$ group had a lower growth state compared with the control group and $KCNH2_{wt}$ groups. Green fluorescence, KCNH2 detection; red fluorescence, ATF6 detection and blue fluorescence, nuclear detection. Magnification, ×200. KCHN2, potassium voltage-gated channel subfamily H member 2; ATF6, activating transcription factor 6; control, normal 293 cells; $KCNH2_{wt}$, 293 cells with transiently expression of wild-type KCNH2; $KCNH2_{A561V}$, transfection of A561V mutant KCNH2 in 293 normal cells; $KCNH2_{wt}$+$KCNH2_{A561V}$ groups, transfection of A561V mutant KCNH2 and wild-type KCNH2 plasmids into 293 cells; wt, wild-type.

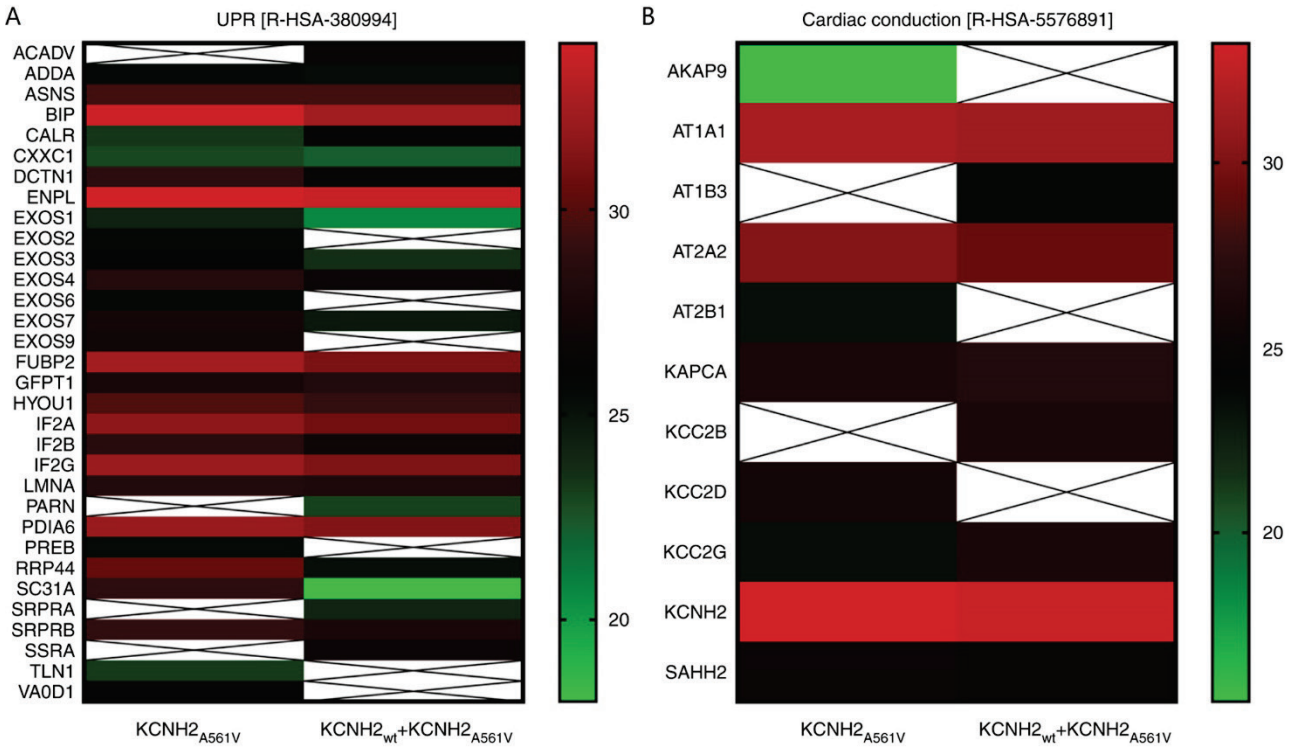

Fig. 4. Thermogram of UPR and cardiac conduction related proteins in immunocoprecipitation samples of $KCNH2_{wt}$+$KCNH2_{A561V}$ group and $KCNH2_{A561V}$ group. (**A**) UPR; (**B**) cardiac-related proteins. The abundance of UPR related proteins in the $KCNH2_{A561V}$ group was higher compared with the $KCNH2_{wt}$+$KCNH2_{A561V}$ group, there was no significant difference between the $KCNH2_{wt}$+$KCNH2_{A561V}$ group and the $KCNH2_{A561V}$ group in cardiac conduction-related proteins. Scale value is the index with abundance value based on 2, the white squares indicate that the corresponding protein was not detected. Red represents the highest and green represents the lowest specificity of differentially expressed genes. KCHN2, potassium voltage-gated channel subfamily H member 2; ATF6, activating transcription factor 6; $KCNH2_{A561V}$, transfection of A561V mutant KCNH2 in 293 normal cells; $KCNH2_{wt}$+$KCNH2_{A561V}$ groups, transfection of A561V mutant KCNH2 and wild-type KCNH2 plasmids into 293 cells; wt, wild-type; UPR, unfolded protein response.

Table 2. GO classification and enrichment analysis.

GO biological process	**GO term**	**BP Components**	**Enrichment Score**	**FDR**	**Enriched Genes**
Cysteine biosynthetic process	GO:0019344	4	2	0.0435	P35520, P0DN79
Positive regulation of histone H2B ubiquitination	GO:2001168	4	2	0.0431	O75150, Q5VTR2
Hydrogen sulfide biosynthetic process	GO:0070814	4	2	0.0428	P35520, P0DN79
Positive regulation of cytoplasmic translation	GO:2000767	11	3	0.0085	P62633, P16989, Q9Y5A9
Negative regulation of nucleocytoplasmic transport	GO:0046823	21	3	0.0314	P46060, P12270, P10599
Mitotic spindle checkpoint	GO:0071174	26	3	0.0429	Q13123, P53350, P12270
Negative regulation of mitotic metaphase/anaphase transition	GO:0045841	28	3	0.0488	Q13123, P53350, P12270
Regulation of mRNA 3'-end processing	GO:0031440	29	3	0.0509	O75150, Q6P1J9, Q5VTR2

FDR, false discovery rate; GO, gene ontology; BP, biological process.

Table 3. Ranking list of GO analysis according to FDR.

GO biological process	GO term	BP Components	Enrichment Score	FDR	Enriched Genes
Positive regulation of cytoplasmic translation	GO:2000767	11	3	0.0085	P62633, P16989, Q9Y5A9
Negative regulation of nucleocytoplasmic transport	GO:0046823	21	3	0.0314	P46060, P12270, P10599
Hydrogen sulfide biosynthetic process	GO:0070814	4	2	0.0428	P35520, P0DN79
Mitotic spindle checkpoint	GO:0071174	26	3	0.0429	Q13123, P53350, P12270
Positive regulation of histone H2B ubiquitination	GO:2001168	4	2	0.0431	O75150, Q5VTR2
Cysteine biosynthetic process	GO:0019344	4	2	0.0435	P35520, P0DN79
Negative regulation of mitotic metaphase/anaphase transition	GO:0045841	28	3	0.0488	Q13123, P53350, P12270
Regulation of mRNA 3'-end processing	GO:0031440	29	3	0.0509	O75150, Q6P1J9, Q5VTR2

FDR, false discovery rate; GO, gene ontology; BP, biological process.

Discussion

KCNH2 is transcribed into an mRNA in the nucleus, transferred to ribosomes in the ER for processing to form an original peptide chain, then core-glycosylated in the ER to produce a precursor with a size of 135 kDa [7]. The core-glycosylated KCNH2 channel protein transfers to contact with the ER-Golgi intermediate compartment and reaches the Golgi body to undergo complete glycosylation, as a result, a 155 kDa mature channel protein forms and enters the cell membrane to perform its function [27-29]. In the present study, the total protein expression of KCNH2 was high in the $KCNH2_{A561V}$ and $KCNH2_{wt}$+$KCNH2_{A561V}$ groups compared with the $KCNH2_{wt}$ group. In addition, the bands representing the complete glycosylation of KCNH2 with a molecular weight of 155 kDa almost disappeared in $KCNH2_{A561V}$ group, and has a slightly increase in $KCNH2_{wt}$+$KCNH2_{A561V}$ group, but has a minimum function due to dominant negative suppression as reported previously. Consequently, the ratio of 155 kDa to 135 kDa decreased significantly in $KCNH2_{A561V}$ and $KCNH2_{wt}$+$KCNH2_{A561V}$ groups compared with $KCNH2_{wt}$. Furthermore, our previous electrophysiological data showed that no tail current was observed in $KCNH2_{A561V}$ group but this was present in $KCNH2_{wt}$+$KCNH2_{A561V}$ group, smaller compared to $KCNH2_{wt}$ group [30]. Hence, our study demonstrated that the *A561V* mutant of KCNH2 inhibited the glycosylation and maturation of the protein.

ATF6 is a type II ER transmembrane protein containing 670 amino acids. Its N-terminal is located in the cytoplasm and it is composed of a basic zinc finger structure DNA transcriptional activation domain [21]. The C-terminal is located in the ER and can sense ERS. It has multiple binding immunoglobulin protein (BIP/GRP78) binding sites and 2 Golgi localization signals (GLS) [31]. A BIP can form a stable complex by combining the GLS region of ATF6 to change its location into the ER and develop an inactive state under normal conditions [32]. However, BIPs bind to these proteins to prevent them from clustering and promote their correct folding when incompletely folded proteins accumulate in the ER and cause ERS; alternately, BIP and GLS are separated, resulting in the transfer of ATF6 out of the ER and into the Golgi complex [33]. In the Golgi apparatus, the N-terminal fragment of ATF6 with a size of ~50 kDa is cleaved and enters the nucleus to serve the role of a transcription factor; hence, the transcription levels of ERS-related proteins, protein-folding chaperones and folding enzymes, such as Bip, IRE1 and GRP78, improve [34].

In the present study, the mRNA expression levels of *ATF6* in the $KCNH2_{wt}$+$KCNH2_{A561V}$ group were higher compared with the $KCNH2_{A561V}$ group, but the full-length protein expression of ATF6 was inhibited. The N-terminal fragment of ATF6 with a UPR regulatory

activity activated by the ER was not detected in the present study. Hence, ATF6 was highly activated, and a large number of ATF6 were sheared in the $KCNH2_{wt}$+$KCNH2_{A561V}$ group (Fig. 3). Consequently, although the ATF6 mRNA expression increased, the full-length protein expression decreased.

hLQTS is a cardiac electrophysiological condition induced by cardiac ion channels disorder that is closely associated with fatal ventricular arrhythmias. Reductions in these ion channels can lead to electrical remodeling and arrhythmias *via* cardiac conduction abnormality. Previous studies shown that inhibition of UPR reduces arrhythmias *via* cardiac conduction related proteins [35]. In our study, a total of 92 UPR (R-HSA-380994)-related proteins are known. Among them, 32 were detected in the present study. RNA exosome complex proteins (UPR-related proteins) are involved in numerous RNA cleavage and degradation activities in cells including the processing of ribosomal and small nucle(ol)ar RNAs and the degradation of mRNAs [36]. The expression level of the RNA exosome complex protein in the $KCNH2_{A561V}$ group was higher compared with the $KCNH2_{wt}$+$KCNH2_{A561V}$ group in the present study. Of the 140 identified cardiac conduction-related proteins (R-HSA-5576891), 11 were detected in the present study, accounting for <0.08 of the total related proteins. In addition, proteomic analysis demonstrated that the abundance of UPR-related proteins in the $KCNH2_{A561V}$ group was higher compared with the $KCNH2_{wt}$+$KCNH2_{A561V}$ group. The activity of GO:0019344 (Cysteine biosynthesis) and GO:2000767 (Positive regulation of protein translation in cytoplasm) process in the $KCNH2_{A561V}$ group was higher compared with the $KCNH2_{wt}$+$KCNH2_{A561V}$ group in the present study.

PERK can inhibit protein translation by phosphorylating elf2 under ERS [37]. PERK activation can also promote the transfer of ATF4 into the nucleus and participate in transcriptional regulation, whereas the downstream gene of ATF4 (cystathionine γ-lyase) can regulate amino acid metabolism. It has been demonstrated that the PERK/elf2/ATF4 pathway is essential not only for translational control, but also for activation of ATF6 and its target genes. Thus, the PERK pathway facilitates both the synthesis of ATF6 and trafficking of ATF6 from the ER to the Golgi for intramembrane proteolysis and activation of ATF6 [38]. In the present study, although ATF6 activation level was higher and UPR was more active in the $KCNH2_{wt}$+$KCNH2_{A561V}$ group compared with the $KCNH2_{A561V}$ group, the crosstalk between PERK/elf2/ATF4 signaling pathway and ATF6 has yet to be investigated. We will explore it through a variety of trials in the future.

Conclusions

The present study demonstrated that the activation level of ATF6 increased significantly and protein translation and synthesis were inhibited when the wild-type and *A561V* mutant of KCNH2 co-expressed. The *A561V* heterozygous mutation of KCNH2 inhibited the protein expression of mature KCNH2 through the UPR mediated by ATF6. These results provided a theoretical basis for clinical treatment of Long QT syndrome.

Conflict of Interest

There is no conflict of interest.

Acknowledgements

This study was supported by Ningbo Natural Science Foundation (No. 2018A610398 and 2022J039, 2022J266), The Medical and Health Research Project of Zhejiang Province (No. 2022KY343) and The Science and Technology Program for Public wellbeing of Ningbo (2022AS069).

References

1. Shah SR, Park K, Alweis R. Long QT Syndrome: A Comprehensive Review of the Literature and Current Evidence. Curr Probl Cardiol 2019;44:92-106. https://doi.org/10.1016/j.cpcardiol.2018.04.002
2. Wallace E, Howard L, Liu M, O'Brien T, Ward D, Shen S, Prendiville T. Long QT Syndrome: Genetics and Future Perspective. Pediatr Cardiol 2019;40:1419-1430. https://doi.org/10.1007/s00246-019-02151-x
3. Neira V, Enriquez A, Simpson C, Baranchuk A. Update on long QT syndrome. J Cardiovasc Electrophysiol 2019;30:3068-3078. https://doi.org/10.1111/jce.14227

4. Restivo M, Caref EB, Kozhevnikov DO, El-Sherif N. Spatial dispersion of repolarization is a key factor in the arrhythmogenicity of long QT syndrome. J Cardiovasc Electrophysiol 2004;15:323-331. https://doi.org/10.1046/j.1540-8167.2004.03493.x
5. Kapplinger JD, Giudicessi JR, Ye D, Tester DJ, Callis TE, Valdivia CR, Makielski JC, ET AL. Enhanced Classification of Brugada Syndrome-Associated and Long-QT Syndrome-Associated Genetic Variants in the SCN5A-Encoded Na(v)1.5 Cardiac Sodium Channel. Circ Cardiovasc Genet 2015;8:582-595. https://doi.org/10.1161/CIRCGENETICS.114.000831
6. Li G, Shi R, Wu J, Han W, Zhang A, Cheng G, Xue X, Sun C. Association of the hERG mutation with long-QT syndrome type 2, syncope and epilepsy. Mol Med Rep 2016;13:2467-2475. https://doi.org/10.3892/mmr.2016.4859
7. Vandenberg JI, Perry MD, Perrin MJ, Mann SA, Ke Y, Hill AP. hERG K(+) channels: structure, function, and clinical significance. Physiol Rev 2012;92:1393-1478. https://doi.org/10.1152/physrev.00036.2011
8. Niven JE, Vahasoyrinki M, Kauranen M, Hardie RC, Juusola M, Weckstrom M. The contribution of Shaker K+ channels to the information capacity of Drosophila photoreceptors. Nature 2003;421:630-634. https://doi.org/10.1038/nature01384
9. Shimizu W. The long QT syndrome: therapeutic implications of a genetic diagnosis. Cardiovasc Res 2005;67:347-356. https://doi.org/10.1016/j.cardiores.2005.03.020
10. Wang Y, Shen T, Fang P, Zhou J, Lou K, Cen Z, Qian H, ET AL. The role and mechanism of chaperones Calnexin/Calreticulin in which ALLN selectively rescues the trafficking defective of HERG-A561V mutation. Biosci Rep 2018;38:BSR20171269. https://doi.org/10.1042/BSR20171269
11. Curran ME, Splawski I, Timothy KW, Vincent GM, Green ED, Keating MT. A molecular basis for cardiac arrhythmia: HERG mutations cause long QT syndrome. Cell 1995;80:795-803. https://doi.org/10.1016/0092-8674(95)90358-5
12. Kagan A, Yu Z, Fishman GI, McDonald TV. The dominant negative LQT2 mutation A561V reduces wild-type HERG expression. J Biol Chem 2000;275:11241-11248. https://doi.org/10.1074/jbc.275.15.11241
13. Tester DJ, Will ML, Haglund CM, Ackerman MJ. Compendium of cardiac channel mutations in 541 consecutive unrelated patients referred for long QT syndrome genetic testing. Heart Rhythm 2005;2:507-517. https://doi.org/10.1016/j.hrthm.2005.01.020
14. Ma S, Zhao Y, Cao M, Sun C. Human etheragogorelated gene mutation L539fs/47hERG leads to cell apoptosis through the endoplasmic reticulum stress pathway. Int J Mol Med 2019;43:1253-1262. https://doi.org/10.3892/ijmm.2019.4049
15. Kim I, Xu W, Reed JC. Cell death and endoplasmic reticulum stress: disease relevance and therapeutic opportunities. Nat Rev Drug Discov 2008;7:1013-1030. https://doi.org/10.1038/nrd2755
16. Bertolotti A, Zhang Y, Hendershot LM, Harding HP, Ron D. Dynamic interaction of BiP and ER stress transducers in the unfolded-protein response. Nat Cell Biol 2000;2:326-332. https://doi.org/10.1038/35014014
17. Yuan ZL, Zhang ZX, Mo YZ, Li DL, Xie L, Chen MH. Inhibition of extracellular signal-regulated kinase downregulates endoplasmic reticulum stress-induced apoptosis and decreases brain injury in a cardiac arrest rat model. Physiol Res 29;71:413-423. https://doi.org/10.33549/physiolres.934882
18. Estebanez B, de Paz JA, Cuevas MJ, Gonzalez-Gallego J. Endoplasmic Reticulum Unfolded Protein Response, Aging and Exercise: An Update. Front Physiol 2018;9:1744. https://doi.org/10.3389/fphys.2018.01744
19. Senft D, Ronai ZA. UPR, autophagy, and mitochondria crosstalk underlies the ER stress response. Trends Biochem Sci 2015;40:141-148. https://doi.org/10.1016/j.tibs.2015.01.002
20. Yoshida H, Okada T, Haze K, Yanagi H, Yura T, Negishi M, Mori K. Endoplasmic reticulum stress-induced formation of transcription factor complex ERSF including NF-Y (CBF) and activating transcription factors 6alpha and 6beta that activates the mammalian unfolded protein response. Mol Cell Biol 2001;21:1239-1248. https://doi.org/10.1128/MCB.21.4.1239-1248.2001
21. Glembotski CC, Rosarda JD, Wiseman RL. Proteostasis and Beyond: ATF6 in Ischemic Disease. Trends Mol Med 2019;25:538-550. https://doi.org/10.1016/j.molmed.2019.03.005
22. Glembotski CC. Roles for ATF6 and the sarco/endoplasmic reticulum protein quality control system in the heart. J Mol Cell Cardiol 2014;71:11-15. https://doi.org/10.1016/j.yjmcc.2013.09.018

23. Ryoo HD. Long and short (timeframe) of endoplasmic reticulum stress-induced cell death. FEBS J 2016;283:3718-3722. https://doi.org/10.1111/febs.13755
24. Bahar E, Kim JY, Yoon H. Quercetin attenuates manganese-induced neuroinflammation by alleviating oxidative stress through regulation of apoptosis, iNOS/NF-kappaB and HO-1/Nrf2 pathways. Int J Mol Sci 2017;18:1989. https://doi.org/10.3390/ijms18091989
25. Livak KJ, Schmittgen TD. Analysis of relative gene expression data using real-time quantitative PCR and the 2(-Delta Delta C(T)) Method. Methods 2001;25:402-408. https://doi.org/10.1006/meth.2001.1262
26. Gardner BM, Pincus D, Gotthardt K, Gallagher CM, Walter P. Endoplasmic reticulum stress sensing in the unfolded protein response. Cold Spring Harb Perspect Biol 2013;5:a013169. https://doi.org/10.1038/nrneph.2017.129
27. Gong Q, Anderson CL, January CT, Zhou Z. Role of glycosylation in cell surface expression and stability of HERG potassium channels. Am J Physiol Heart Circ Physiol 2002;283:H77-H84. https://doi.org/10.1152/ajpheart.00008.2002
28. Zhang KP, Yang BF, Li BX. Translational toxicology and rescue strategies of the hERG channel dysfunction: biochemical and molecular mechanistic aspects. Acta Pharmacol Sin 2014;35:1473-1484. https://doi.org/10.1038/aps.2014.101
29. Foo B, Williamson B, Young JC, Lukacs G, Shrier A. hERG quality control and the long QT syndrome. J Physiol 2016;594:2469-2481. https://doi.org/10.1113/JP270531
30. Wu Y, Huang X, Zheng Z, Yang X, Ba Y, Lian J. Role and mechanism of chaperones calreticulin and ERP57 in restoring trafficking to mutant HERG-A561V protein. Int J Mol Med 2021;48:159. https://doi.org/10.3892/ijmm.2021.4992
31. Hong M, Luo S, Baumeister P, Huang JM, Gogia RK, Li M, Lee AS. Underglycosylation of ATF6 as a novel sensing mechanism for activation of the unfolded protein response. J Biol Chem 2004;279:11354-11363. https://doi.org/10.1074/jbc.M309804200
32. Shen J, Chen X, Hendershot L, Prywes R. ER stress regulation of ATF6 localization by dissociation of BiP/GRP78 binding and unmasking of Golgi localization signals. Dev Cell 2002;3:99-111. https://doi.org/10.1016/S1534-5807(02)00203-4
33. Shen J, Prywes R. ER stress signaling by regulated proteolysis of ATF6. Methods 2005;35:382-389. https://doi.org/10.1016/j.ymeth.2004.10.011
34. Ye J, Rawson RB, Komuro R, Chen X, Dave UP, Prywes R, Brown MS, Goldstein JL. ER stress induces cleavage of membrane-bound ATF6 by the same proteases that process SREBPs. Mol Cell 2000;6:1355-1364. https://doi.org/10.1016/S1097-2765(00)00133-7
35. Liu M, Liu H, Parthiban P, Kang GJ, Shi G, Feng F, Zhou A, ET AL. Inhibition of the unfolded protein response reduces arrhythmia risk after myocardial infarction. J Clin Invest 2021;131:e147836. https://doi.org/10.1172/JCI147836
36. van Dijk EL, Schilders G, Pruijn GJ. Human cell growth requires a functional cytoplasmic exosome, which is involved in various mRNA decay pathways. RNA 2007;13:1027-1035. https://doi.org/10.1261/rna.575107
37. Rozpedek W, Pytel D, Mucha B, Leszczynska H, Diehl JA, Majsterek I. The role of the PERK/eIF2alpha/ATF4/CHOP signaling pathway in tumor progression during endoplasmic reticulum stress. Curr Mol Med 2016;16:533-544. https://doi.org/10.2174/1566524016666160523143937
38. Teske BF, Wek SA, Bunpo P, Cundiff JK, McClintick JN, Anthony TG, Wek RC. The eIF2 kinase PERK and the integrated stress response facilitate activation of ATF6 during endoplasmic reticulum stress. Mol Biol Cell 2011;22:4390-4405. https://doi.org/10.1091/mbc.e11-06-0510